

Numerical Simulation of Turbulent Air Flows in Aseptic Clean Rooms

Eleonora Bottani, Roberto Rizzo and Giuseppe Vignali
*Department of Industrial Engineering, University of Parma
 Italy*

1. Introduction

Sterile air condition is an increasingly important requirement, as several manufacturing processes, such as food production, preparation of aseptic products for the pharmaceutical industry, manufacturing of microelectronics components, compact discs and photographic films, need optimal air cleaning.

Aseptic clean rooms were developed to satisfy the above requirement. According to Wirtanen et al. (2002), a clean room can be defined as “a room in which the concentration of airborne particles is controlled, and which is constructed and used in a manner to minimize the introduction, generation, and retention of particles inside the room, and in which other relevant parameters, e.g. temperature, humidity, and pressure, are controlled as necessary”. The objective of clean room technology in various clean room classes in the food and beverage industry is to ensure the control of contaminants in sensitive processes. Use of this technology should be considered in processes where microbial inactivation, e.g. through thermal sterilization or deep freezing, is not feasible. If critical process risks are identified due to exposure of the product to airborne microbes during processing or if severe sedimentation of airborne microbes can occur on critical process surfaces, clean room technology can be used to solve the problems (Schicht, 1999; Whyte, 2001). In an aseptic clean room, the air flow, properly filtered, is flushed from the top of the chamber to special grids placed at the bottom of the structure. Then, it is recirculated by an air filtering unit; here, part of the air flow is ejected and replaced by external air that will undergo filtration. A main requirement of clean rooms is that they are maintained at a pressure higher than the external one, to prevent pollutants air flow from the environment.

Currently accepted standards describing clean rooms are developed by the Federal Standard (Federal Standard 209 E, 1992) and adopted by ISO (2006); such standards suggest an international classification of clean rooms, based on thirteen possible classes depending on the maximum allowed number of pollutant particles in the room. Eq.1 provides an empirical relation between the aseptic class M and the diameter of the pollutant particles d [mm] in the room:

$$\text{Particles/m}^3 = 10 M (0.5/d)^{2.2} \quad (1)$$

When designing an aseptic room, special care should be taken to ensure a well distributed flow of relatively dry, high-efficiency particulate air (HEPA) filtered air along walls,

windows and ceiling. Due to its characteristics, the aseptic room can involve laminar unidirectional or turbulent non-unidirectional air flows. In both cases, air flow within the clean room area is an important factor in the precise control of air over the container into which food products are assembled (Wirtanen et al., 2002).

Previous studies have examined several aspects of the air flow in the clean room, such as the influence of air velocity on contamination control as a function of room characteristics (e.g. Ogawa, 2000) or factors affecting airflow in clean rooms (e.g. Fitzpatrick, 1994). Moreover, in the last decade, many research works proposed numerical models to predict the clean room air flow (Divelbiss & Winter, 1995; Cheng et al., 1999; Chen et al., 2007). Thanks to the increasing performance of PC, the numerical analysis of the flow behavior inside indoor environments became more detailed and refined. In particular, several commercial CFD packages allow analyzing 3-dimensional fields using several solver methods (Norton & Sun, 2006).

In this chapter, we focus on developing a simulation model to reproduce and analyze the flow of sterile air within an aseptic clean room in the case of a non-unidirectional fluid flow. The analyzed clean room is used in aseptic beverage bottling, to perform sterilization of bags containing High Density Poly-Ethylene (HDPE) caps, by flushing hydrogen peroxide vapor. Hence, the analysis carried out aims at developing a tool that can be usefully exploited to improve the sterilization ability of the aseptic clean rooms at the design phase, with a particular focus on optimizing sterile air circulation inside the room.

This chapter is organized as follows. In the next section, we provide some theoretical fundamentals about turbulent flow modeling. To adequately reproduce the turbulent air flows in the aseptic room and to ensure correspondence with real aseptic plants, in developing the simulation tool two possible turbulence models are considered, namely the $k-\epsilon$ (Launder & Spalding, 1974) and the $k-\omega$ (Wilcox, 1988) models, which are detailed in that section. Then, the model developed and the settings are presented. In section 4, we provide validation of the model based on experimental data and analyze the turbulent flow behavior. In the conclusion section a brief discussion about the two turbulence models adopted and future research directions are presented.

2. Turbulent flow modeling

2.1 Introduction

A turbulent flow is a chaotic process, which is difficult to describe in details. For this purpose, Reynolds (1883) introduced a decomposition of the flow parameters, considering average values and their fluctuation, this latter resulting from turbulence. Based on this approach, a generic parameter φ can be quantified starting from its average value Φ measured during a defined time interval Δt , and its fluctuating part, i.e.:

$$\varphi = \varphi'(t) + \Phi \quad (2)$$

Both components of φ can be obtained from averaging equations, usually referred to as "Reynolds Averaging Navier-Stokes" (RANS) equations, resulting from the integration in time of the parameter examined. The integration time T ("averaging time") should be carefully chosen, to be sufficiently larger than the turbulent time interval, but at the same time small enough so as relevant information about the fluctuation of the fluid in time is not missed.

Following eq.2, the instantaneous velocity of a point $u_i(\bar{x},t)$ can be written as the sum of an average value $\bar{u}_i(\bar{x})$ and a variable one $u_i'(\bar{x},t)$, according to the following formula:

$$u_i(\bar{x},t) = \bar{u}_i(\bar{x}) + u_i'(\bar{x},t) \tag{3}$$

where $\bar{u}_i(\bar{x})$, in turn, is defined as:

$$\bar{u}_i(\bar{x}) = \frac{1}{T} \int_t^{t+T} u_i(\bar{x},t) dt \tag{4}$$

being T the averaging time. Some of the properties of the above formulae are described in the following equations:

$$\overline{\bar{u}_i(\bar{x})} = \frac{1}{T} \int_t^{t+T} \bar{u}_i(\bar{x}) dt = \bar{u}_i(\bar{x}) \tag{5}$$

$$\overline{u_i'(\bar{x},t)} = 0 \tag{6}$$

Hence, the average of the $\bar{u}_i(\bar{x})$ parameter equals the average of the velocity $u_i(\bar{x},t)$, and the average value of the fluctuating component $u_i'(\bar{x},t)$ is null.

Applying the averaging approach to the mass equation, the following formula is derived:

$$0 = \frac{\partial \bar{\rho}}{\partial t} + \frac{\partial \bar{\rho} \bar{u}_i}{\partial x_i} + \frac{\partial \overline{\rho' u_i'}}{\partial x_i} \tag{7}$$

From eq.7, it can be seen that a new parameter $\overline{\rho' u_i'}$ should be added in the computation. To derive the fluctuations in density, in the case of compressible fluids, the approach proposed by Favre (1969), suggests computing the weighted average of velocity, being weight the fluid density. Eq.8 summarises the computation:

$$\tilde{u}_i(\bar{x}) = \frac{1}{\bar{\rho}} \int \rho(\bar{x},t) u_i(\bar{x},t) dt \tag{8}$$

where $\bar{\rho}$ [kg/m³] is the average value of density computed according to Reynolds (1883). Moreover, the velocity $u_i(\bar{x},t)$ can be rewritten as:

$$u_i(\bar{x},t) = \tilde{u}_i(\bar{x}) + u_i''(\bar{x},t) \tag{9}$$

Combining the above formula with eq.7, the following expressions are derived:

$$\frac{\partial \bar{\rho}}{\partial t} + \frac{\partial \bar{\rho} \cdot \tilde{u}_i}{\partial x_i} = 0 \tag{10}$$

$$\frac{\partial(\bar{\rho} \cdot \tilde{u}_i)}{\partial t} + \frac{\partial(\bar{\rho} \cdot \tilde{u}_i \cdot \tilde{u}_j)}{\partial x_j} = -\frac{\partial \bar{p}}{\partial x_i} + \frac{\partial(\mu \cdot \nabla \tilde{u}_i)}{\partial x_j} - \frac{\partial(\overline{\rho' \cdot u_i'' \cdot u_j''})}{\partial x_j} + S_{M_i} \tag{11}$$

The above equations can be solved applying the average values defined by Favre (1969), except the $\overline{\rho' \cdot u_i'' \cdot u_j''}$ parameter, known as Reynolds "stress", which should be defined

starting from the boundary conditions of the case examined. In the case of turbulent flows, in particular, all terms should be modelled to derive a solution describing the average values of the fluid motion. To this extent, several turbulence models were proposed, whose applicability depends on the level of detail required and on the value of the Reynolds number.

Turbulence models grounds on the assumption that, under high Reynolds number, the fluid energy substantially increases, and could not be dissipated during flow; hence, the fluid experiences a macroscopic destabilization, which leads to vortices formation and to energy transfer from larger to smaller vortices. Under this flow regime, the system can be described by the energy transfer between vortices, which is measured by means of the dissipation ε [m^2/s^3] and by the turbulent kinetic energy k [J/kg]. The formal definition of ε is provided by the following equation:

$$\varepsilon = \frac{u'^2}{L} \quad (12)$$

being L [m] the length measurement scale and u' [m/s^2] the fluctuation of the velocity in time. The Reynolds number referred to the measurement scale of the above system is defined as:

$$R_{eL} = \frac{u' L}{\nu} \quad (13)$$

being ν [m^2/s] the kinematic viscosity of the fluid. During energy transfer, the Reynolds number R_{eL} significantly decreases, reaching values close to one, this latter corresponding to the situation where inertia and viscous forces are almost balanced. The Kolmogorov scale η_k (Kolmogorov, 1941) was introduced to identify microscopic turbulent flows that occur in this latter case; the scale is defined as:

$$\eta_k = \left(\frac{\nu^3}{\varepsilon} \right)^{\frac{3}{4}} \quad (14)$$

and corresponds to a unitary Reynolds number, according to the following computation:

$$R_{e\eta k} = \frac{\varepsilon^{\frac{1}{3}} \eta_k^{\frac{4}{3}}}{\nu} = 1 \quad (15)$$

The ratio between macroscopic and microscopic flows can be expressed as:

$$\frac{L}{\eta_k} = R_{eL}^{\frac{3}{4}} \quad (16)$$

2.2 Two-equation turbulence models

In most practical cases, eq.11 is solved applying turbulence models grounded on the Boussinesq assumption (Rajagopal et al., 1996), stating that Reynolds "stress" can be expressed as per the following formula:

$$-\overline{\rho u_i u_j} = \mu_t \left(\frac{\partial u_i}{\partial x_j} + \frac{\partial u_j}{\partial x_i} \right) - \frac{2}{3} \left(\rho k + \mu_t \frac{\partial u_i}{\partial x_i} \right) \delta_{ij} \tag{17}$$

Eq.17 describes the Reynolds “stress” based on a fluctuating value, which is related to the average value by introducing the turbulent viscosity μ_t [kg/m²/s].

Two-equation models are all grounded on the equation describing the transport of kinetic energy k , and on an additional formula, describing a further system characteristic. In this chapter, we focus on models describing either the dissipation ε or the specific dissipation rate ω [1/s]. Such models have emerged from the literature as the most widely adopted in similar studies (Kuznik et al., 2007).

The standard k - ε model

The k - ε model (Launder & Spalding, 1974) is one of the most widely adopted approaches for turbulent flow simulation under commercial software packages. In this model, the turbulent viscosity μ_t is computed according to the following formula:

$$\mu_t = \rho C_\mu \frac{k^2}{\varepsilon} \tag{18}$$

where the kinetic energy k and the dissipation ε are derived from the resolution of the following set of equations:

$$\frac{\partial}{\partial x_j} (\rho u_j k) = \frac{\partial}{\partial x_j} \left[\frac{\mu_{eff}}{\sigma_k} \frac{\partial k}{\partial x_j} \right] + \mu_t \left(\frac{\partial u_i}{\partial x_j} + \frac{\partial u_j}{\partial x_i} \right) \left(\frac{\partial u_i}{\partial x_j} \right) - \rho \varepsilon \tag{19}$$

$$\frac{\partial}{\partial x_j} (\rho u_j \varepsilon) = \frac{\partial}{\partial x_j} \left[\frac{\mu_{eff}}{\sigma_\varepsilon} \frac{\partial \varepsilon}{\partial x_j} \right] + C_{\varepsilon 1} \frac{\varepsilon}{k} \mu_t \left(\frac{\partial u_i}{\partial x_j} + \frac{\partial u_j}{\partial x_i} \right) \left(\frac{\partial u_i}{\partial x_j} \right) - \rho C_{\varepsilon 2} \frac{\varepsilon^2}{k} \tag{20}$$

$$\mu_{eff} = \mu + \mu_t \tag{21}$$

being μ the molecular viscosity, μ_t the turbulent viscosity of the fluid. The C_i and the σ_i parameters are set to the following values: $\sigma_k=0.9$; $\sigma_\varepsilon=1.30$; $C_{\varepsilon 1}=1.44$; $C_{\varepsilon 2}=1.92$; $C_\mu=0.09$ (Cheng et al., 1999).

The standard k - ω model

The k - ω model (Wilcox, 1988) differs from the previous one in that it takes into account the specific dissipation rate ω instead of the dissipation ε . The dissipation rate is defined as a function of the dissipation ε as:

$$\omega = \frac{\varepsilon}{k\beta^*} \tag{22}$$

According to Wilcox (1988), the computation of ω instead of ε allows the model to better reproduce the fluid behavior close to the system boundaries. Eqs.23-25 are exploited in the model to derive the k and ω parameters:

$$\frac{\partial k}{\partial t} + u_j \frac{\partial k}{\partial x_j} = \tau_{ij}^R \frac{\partial \overline{u_i}}{\partial x_j} - \beta^* k \omega + \frac{\partial}{\partial x_j} \left[(\mu + \sigma \mu_t) \frac{\partial k}{\partial x_j} \right] \tag{23}$$

$$\frac{\partial \omega}{\partial t} + u_j \frac{\partial \omega}{\partial x_j} = \alpha \frac{\omega}{k} \tau_{ij}^R \frac{\partial \bar{u}_i}{\partial x_j} - \beta \omega^2 + \frac{\partial}{\partial x_j} \left[(\mu + \sigma \mu_t) \frac{\partial \omega}{\partial x_j} \right] \quad (24)$$

$$\mu_t = \frac{k}{\omega} \quad (25)$$

τ_{ij}^R in eqs.23-24 indicates the components of the Reynolds stress tensor. α , β , β_0 , σ , $\chi_{\omega r}$, $\chi_{k r}$, f_{β} are empirical coefficients whose values are set by the software used for numerical simulations (Comsol Inc., 2005; Wilcox, 1998).

3. Model development

The simulation tool to reproduce the flow of sterile air inside the clean room is based on a Finite Element Method (FEM) numerical model, developed under COMSOL Multiphysics release 3.3 (Comsol Inc.) commercial package. Specifically, the RANS formulation of Navier-Stokes equations (eqs.10-11), implemented in the "Chemical Engineering Module" of COMSOL Multiphysics, is adopted to describe the fluid motion. The simulation model was run on a 2.4 GHz Pentium IV PC, with 2Gb RAM memory, under Windows XP professional platform.

The volume of the clean room examined is 2.786x2.786x1.5 m³. The air flow is flushed in the room from four filters, whose size is 0.61x0.61 m², sited at the top of the chamber. As many exit grids are located on the chamber walls. These latter are partially covered, to ensure that the air flow does not immediately exit the chamber. Figure 1 shows a picture of the chamber geometry developed under COMSOL Multiphysics.

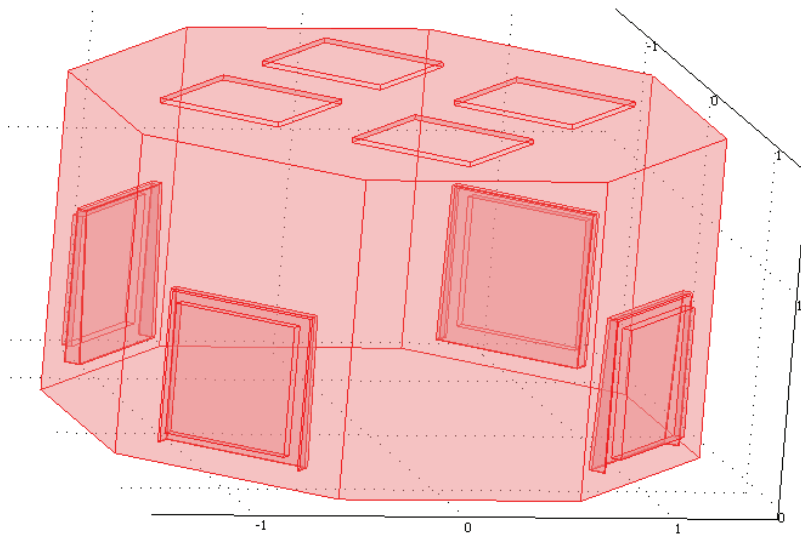


Figure 1. Domain of the model developed

The mesh used to solve the flow equations for the aseptic room consists of 7,555 elements, yielding approximately 66,817 degrees of freedom.

To reduce memory consumption, the GRMES (Generalised Minimum RESidual) indirect iterative solver has been adopted to solve the air flow equations in the aseptic room. Steady state nonlinear analysis and time-dependent iterative solver were exploited to solve the equations of the model.

3.1 k - ε boundary settings

Inlet surfaces

Boundary settings of the k - ε model were defined as follows. For inlet surfaces, a uniform velocity distribution was assumed, whose value U was set to -0.542 m/s along the z -axis (i.e. on the vertical direction). This value, corresponding to the typical velocity of an operating clean room, was derived from the air flow entering the chamber, accounting for $2,900$ m³/h and the surface of the entering grid. k and ε values for the grid surface were set to the following values:

$$k = 1.5 \cdot (U I_T)^2 \quad (26)$$

$$\varepsilon = C_\mu^{0.75} \cdot k^{1.5} / L_T \quad (27)$$

being U the flow velocity [m/s] and $I_T=0.054$ and $L_T=0.07$ the turbulence intensity and length scales, respectively. Numerical values for I_T and L_T were derived from the software user's guide (Comsol Inc., 2005).

Outlet surfaces

For outlet surfaces, we set the atmospheric pressure as boundary condition. Moreover, the following conditions were set for the k and ε values:

$$\mathbf{n} \cdot \nabla k = 0 \quad (28)$$

$$\mathbf{n} \cdot \nabla \varepsilon = 0 \quad (29)$$

Wall surfaces

In the case of turbulent flows in a confined space, numerical results significantly depend on the model settings for surfaces close to the system walls. Those surfaces, in fact, are more likely to be affected by vortices or turbulence formation, resulting in a rapid fluctuation of the model parameters. In this regard, two procedures can be followed to set the model parameters for the system walls. A first approach suggests modifying the model settings so that the flow parameters can be easily computed; in particular, as the model parameters can rapidly change, the number of cells used for the computation should be sufficiently increased, if compared with other points of the domain, to capture those fluctuations. This may correspondingly increase the computational time.

In this study, we follow the "wall function" approach, which suggests keeping the turbulence model unchanged even for surfaces close to the system wall; as a result, the effect of viscous flows is neglected in the computation. Hence, the model setting requires the first mesh nodes to be located at a sufficient distance from the wall, so as for intermediate points the logarithmic wall function can be used for the computation of velocity.

Accordingly, the logarithmic wall function was applied as boundary condition for the room walls; as a result, the normal component of the velocity is set to zero, i.e.:

$$\mathbf{n} \cdot \mathbf{U} = 0 \quad (30)$$

To take into account the tangential component of the velocity U_T , a friction force at the room wall is introduced, which is defined by the following set of equations:

$$\tau_w = \frac{\rho C_\mu^{1/4} k^{1/2}}{\frac{1}{\kappa} \ln(y^+) + C} U_T \quad (31)$$

$$y^+ = \frac{\delta_w \rho C_\mu^{1/4} k^{1/2}}{\eta} \quad (32)$$

being δ_w [m] the distance from the wall and C a parameter describing the surface roughness. The numerical values of those parameters were set to the mesh size (corresponding to the default setting of COMSOL) and to 5.5, respectively. κ is the von Karman constant ($\kappa \approx 0.418$). For the remaining parameters, the logarithmic wall function involves the following boundary conditions:

$$\mathbf{n} \cdot \nabla k = 0 \quad (33)$$

$$\varepsilon = \frac{C_\mu^{3/4} k^{3/2}}{\kappa \delta_w} \quad (34)$$

3.2 k - ω settings

Inlet surfaces

The settings of the k - ω model were defined following a similar procedure. More precisely, as per the previous model, for inlet boundaries a uniform velocity distribution was assumed, with the same numerical value U of -0.542 m/s along the z -axis.

k and ω values for the inlet surfaces were defined based on the following equations:

$$k = 1.5 \cdot (U I_T)^2 \quad (35)$$

$$\omega = \frac{C_\mu^{-0.25} \cdot k^{0.5}}{L_T} \quad (36)$$

where the I_T and L_T parameters were set to the same values of the k - ε model (Comsol Inc., 2005).

Outlet surfaces

As per the previous model, for outlet surfaces, we set the atmospheric pressure as boundary condition. Moreover, the following condition was set for the k and ω values:

$$\mathbf{n} \cdot \nabla k = 0 \quad (37)$$

$$\mathbf{n} \cdot \nabla \omega = 0 \quad (38)$$

Wall surfaces

As per the previous model, the logarithmic wall function was exploited to examine the fluid flow for wall surfaces. Accordingly, the same conditions described in eqs.30 and 33 were

defined in the model. In this case, however, the ω parameter is defined instead of ε . The following equation is adopted to this extent:

$$\omega = \frac{C_{\mu}^{-0.25} k^{0.5}}{\kappa \delta_w} \tag{39}$$

4. Results and discussion

4.1 Data collection

To validate the simulation tool developed, an appropriate experimental campaign has been performed to derive data that could be compared with simulation outcomes provided by the model developed. To collect data, a prototypical aseptic clean room was exploited, available at the production line of an Italian company, manufacturing aseptic bottling plants.

Experimental data collected refer to fluid velocity in 4 locations of the aseptic room, namely:

- (i) the middle zone of the clean room (location A);
- (ii) a point close to the outlet ducts (location B);
- (iii) a point at a defined distance from the outlet ducts (location C); and
- (iv) the middle of the clean room along the z-axis (location D).

To collect the experimental data, the aseptic room was stopped and the sterilizing solution was removed from the chamber, to ensure that the conditions of data collection were as similar as possible to those reproduced by the turbulence model. The measurements of fluid velocity in the areas described above were performed both with a hot-wire anemometer and plate anemometer, both provided by the company. The plate anemometer was especially used when it was necessary to only derive one component of the fluid velocity. In the following, we detail the experimental measurements performed for the above described locations.

Location A

The hot-wire anemometer was initially placed at $(x; y; z)=(0; 0.375; 0.325)$, and moved along the y -axis up to the room center, following the path shown in Figure 2.

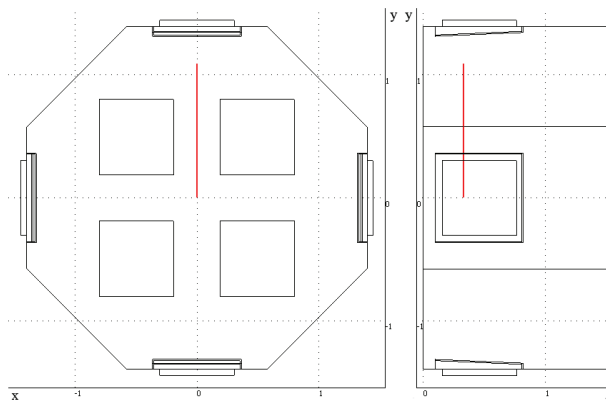


Figure 2. Location A

Location B

The hot-wire anemometer was located close to the outlet grids, as shown by the red line in Figure 3. Data were collected at five different points, whose coordinates are $(x; y; z)=(x_n; 1.363; 0.095)$, with $x_1=-0.335$; $x_2=-0.1775$; $x_3=0$; $x_4=0.1775$; $x_5=0.335$.

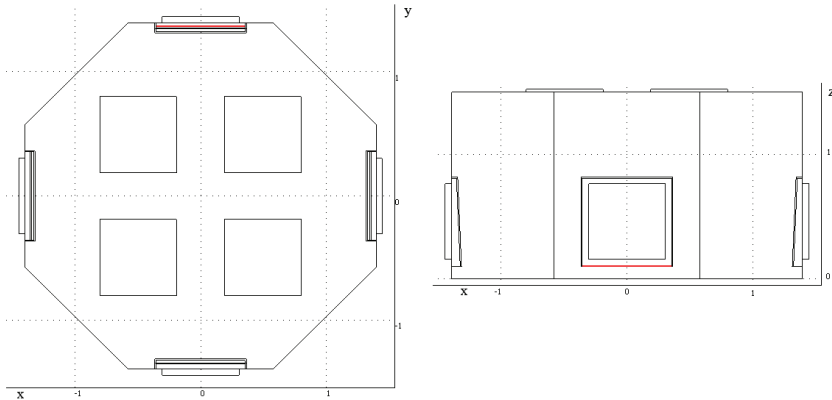


Figure 3. Location B

Location C

The plate anemometer was located 0.237 m far from the outlet grid, at 0.055 m height from the chamber floor, as shown in Figure 4. Data were collected at five different points, whose coordinated are $(x; y; z)=(x_n; 1.086; 0.055)$, with $x_1=-0.335$; $x_2=-0.1775$; $x_3=0$; $x_4=0.1775$; $x_5=0.335$.

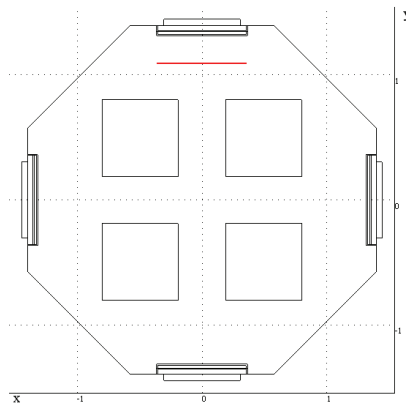


Figure 4. Location C

Location D

As shown in Figure 5, the plate anemometer was located in the middle of one of the inlet grids, at point $(x; y; z)=(0.495; 0.495; z_n)$. Several values of height from the chamber floor were considered, namely $z_1=0.225$; $z_2=0.55$; $z_3=0.875$; $z_4=1.2$; $z_5=1.345$.

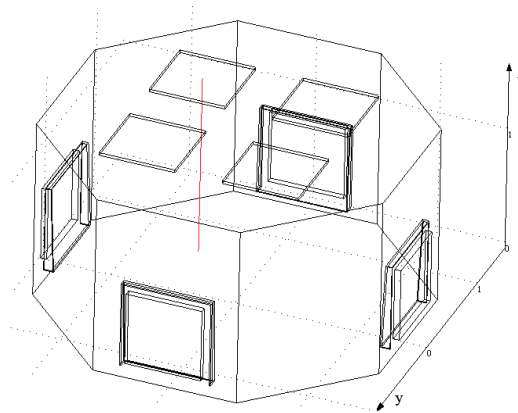


Figure 5. Location D

4.2 Model validation

Figure 6 shows the results of the $k-\epsilon$ model, in terms of both stationary analysis and transitory one, this latter representing the initial 2.8 s of the numerical simulation. By comparing those outcomes, it can be observed that, under transitory conditions, the flow velocity reaches stabilization in time, and assumes values very similar to outcomes of the stationary analysis. Based on this consideration, the results of the stationary analyses were assumed as reference to compare the simulation outcomes with the experimental data.

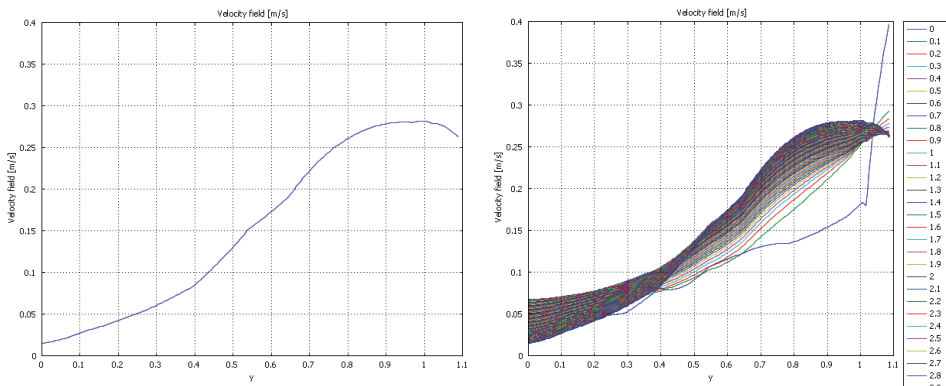


Figure 6. Comparison between transitory and stationary conditions – location A

Detailed results of the numerical models are proposed in Table 1 for both the $k-\epsilon$ and $k-\omega$ models, together with experimental data collected in the locations examined.

Subsequent Figure 7-Figure 10 graphically illustrate the comparison between numerical outcomes and experimental data collected.

	Measurement point [m]	Velocity values [m/s]		
Location A	(x;y;z)=(0;y;0.325)	Experimental	Numerical $k-\epsilon$	Numerical $k-\omega$
	y=0	0.02	0.015	0.21
	y=0.375	0.05	0.077	0.227
	y=0.612	0.15	0.18	0.252
	y=0.849	0.25	0.27	0.285
	y=1.086	0.31	0.27	0.282
Location B	(x;y;z)=(x;1.363;0.095)	Experimental	Numerical $k-\epsilon$	Numerical $k-\omega$
	x=-0.335	4.64	5.41	7.01
	x=-0.1775	3.95	4.7	4.52
	x=0	4.17	3.93	2.65
	x=0.1775	4.35	4.36	4.25
	x=0.335	4.68	6.09	6.55
Location C	(x;y;z)=(x;1.086;0.055)	Experimental	Numerical $k-\epsilon$	Numerical $k-\omega$
	x=-0.335	0.46	0.61	0.697
	x=-0.1775	0.51	0.76	0.643
	x=0	0.56	0.79	0.59
	x=0.1775	0.57	0.76	0.613
	x=0.335	0.49	0.56	0.687
Location D	(x;y;z)=(-0.495;0.495;z)	Experimental	Numerical $k-\epsilon$	Numerical $k-\omega$
	z=0.225	0.34	0.15	0.26
	z=0.55	0.4	0.322	0.282
	z=0.875	0.41	0.451	0.31
	z=1.2	0.48	0.534	0.31
	z=1.345	0.53	0.537	0.475

Table 1. Comparison between experimental and simulated results

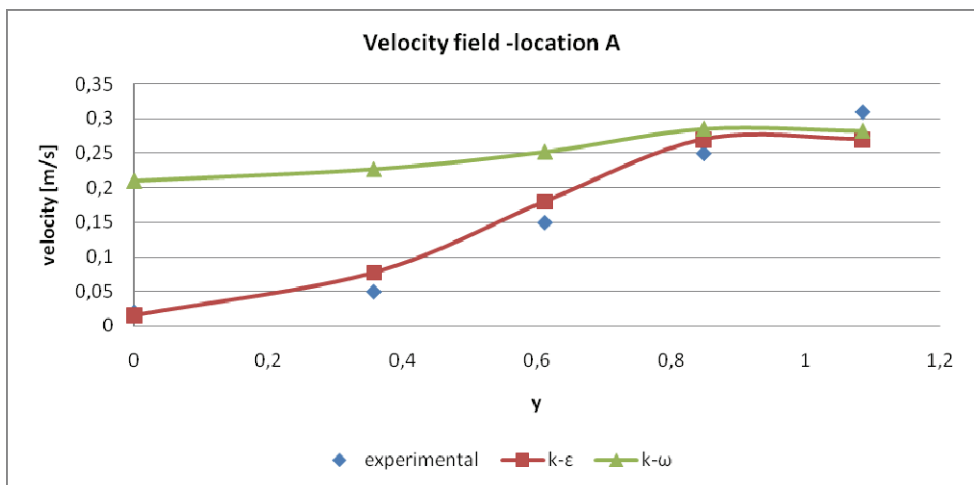


Figure 7. Comparison between experimental and numerical results – location A

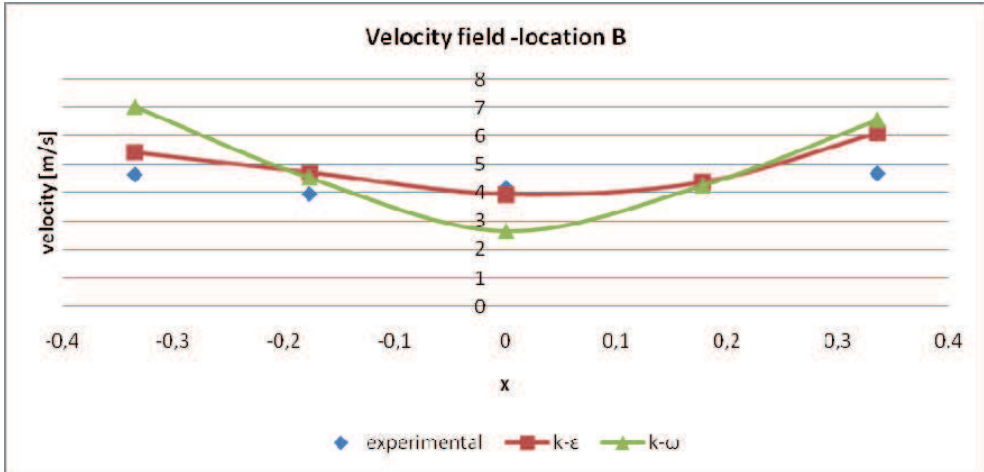


Figure 8. Comparison between experimental and numerical results – location B

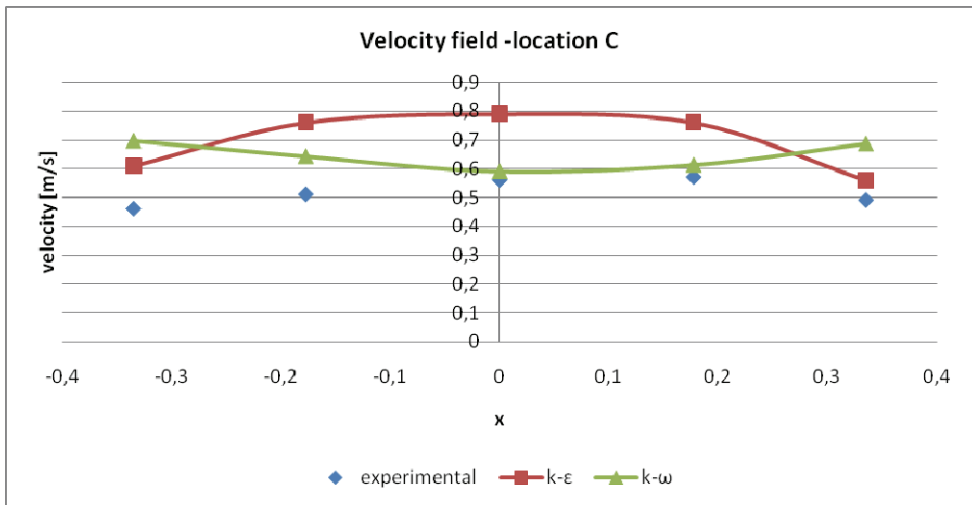


Figure 9. Comparison between experimental and numerical results – location C

The comparison between experimental data and simulation outcomes shows that the $k-\epsilon$ turbulence model is in general able to accurately reproduce the velocity profile observed during experimental measurements. In particular, as can be seen from Figure 7 and Figure 8, location A, corresponding to the central area of the clean room, and location B, corresponding to the outlet grids, show the highest correspondence between experimental and simulated values. In both cases, the simulation outcomes allow correctly reproducing the experimental velocity profile. Conversely, the $k-\omega$ model tends to overestimate the air velocity measured at location A, except for y values greater than about 1 m. Similar considerations can be drawn for location B, where the velocity profile resulting from the $k-\omega$ does not precisely reproduce the experimental data.

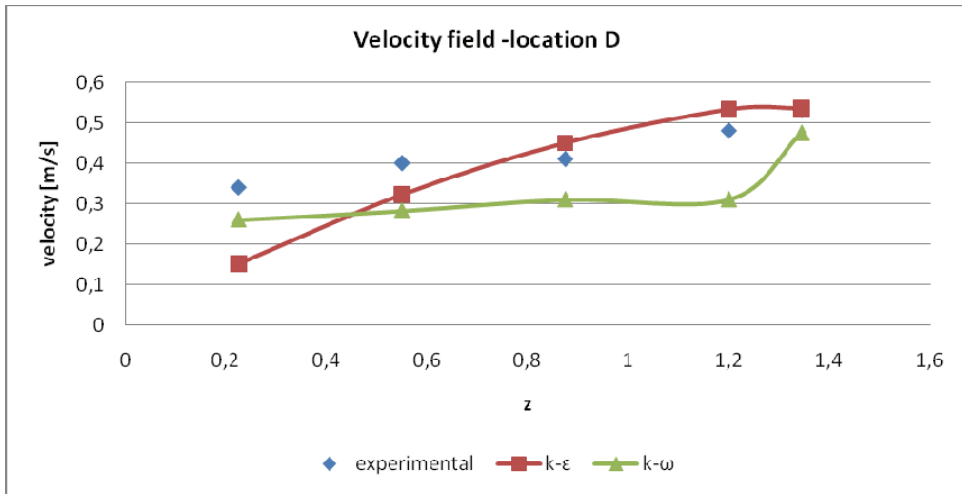


Figure 10. Comparison between experimental and numerical results – location D

Results for location C (see Figure 9) show that the numerical $k-\epsilon$ model slightly overestimates (approx 0.2 m/s) the air velocity in proximity of the outlet grids. This result could be explained considering possible disturbances during the experimental measurements, due to the presence of one or more employees measuring the flow velocity. In addition, due to the presence of the plate, the anemometer used for those measurements does not enable to measure the flow velocity in a precise point, but rather in a zone perpendicular to the plate. This may affect the capability of correctly identifying the height along the z -axis to be assumed as reference to assess the correctness of the simulation results. Conversely, results of the $k-\omega$ model are able to accurately predict the fluid flow only for $0.1775 < x < 0$; for the remaining points, numerical outcomes seem to suggest a trend of flow velocity significantly different from experimental values.

Finally, numerical results for location D (see Figure 10) show that the $k-\epsilon$ model is able to accurately reproduce the air flow in the middle of the clean room only for z values higher than 0.875 m. For lower values, the model seems to slightly underestimate the resulting flow. As per the location C, such a difference could be expected, as the same measurement instrument has been used to derive the fluid flow in location D, resulting in difficult identification of the z value to be assumed as reference to assess the the correctness of the simulation outcomes. Conversely, the $k-\omega$ model seems to better reproduce the velocity profile, although numerical values always underestimate the experimental values.

4.3 Flow analyses

Once the simulation model was developed, the subsequent analyses were focused on examining the fluid flow inside the aseptic clean room, in terms of fluid velocity and pressure, and turbulent kinetic energy. On the basis of the results detailed in the previous section, the $k-\epsilon$ model was exploited to this extent.

Figure 11 shows the simulation results in terms of the velocity field at the centre of the clean room ($x=0$). As can be seen from the figure, the velocity inside the room can range from approx 0.036 m/s to 5 m/s. Velocity values from 3 to 5 m/s, however, are achieved only at

the outlet grids, while the flow velocity inside the clean room is always lower than 1 m/s. This does not necessarily involve laminar flow, as Ljungqvist & Reinmuller, (1997), point out that turbulent flows occur in aseptic clean room even at low speed (0.2 m/s).

On the other hand, low velocity could involve poor air recirculation and not well distributed flow of air in central zone of the chamber, which is a main requirement of clean rooms technology.

Moreover, streamlines in Figure 11 indicate flow recirculation at the top left and right of the chamber. This suggests that the air flow does not immediately exit the clean room, allowing the chamber to be maintained at a pressure higher than the external, and thus preventing pollutants entrance from the environment. Such conclusion is supported by the simulated pressure values resulting inside the clean room; they are detailed in Figure 12 (a) for $x=0$. As can be seen from the figure, the chamber is maintained at approx $1.014 \cdot 10^5$ Pa pressure, which is higher to the external one.

Finally, the turbulent kinetic energy k was examined to assess whether the chamber considered experiences significant turbulence. Figure 12 (b) shows that simulated values of turbulent kinetic energy for the aseptic room examined ranges from $9.37 \cdot 10^{-3}$ to 9.335 J/kg. In particular, highest values are achieved at the centre of the outlet grids, while the body of the chamber highlights kinetic energy values lower than 1 J/kg. This suggests that the aseptic room examined experiences limited turbulence, which is mainly located at the outlet grids.

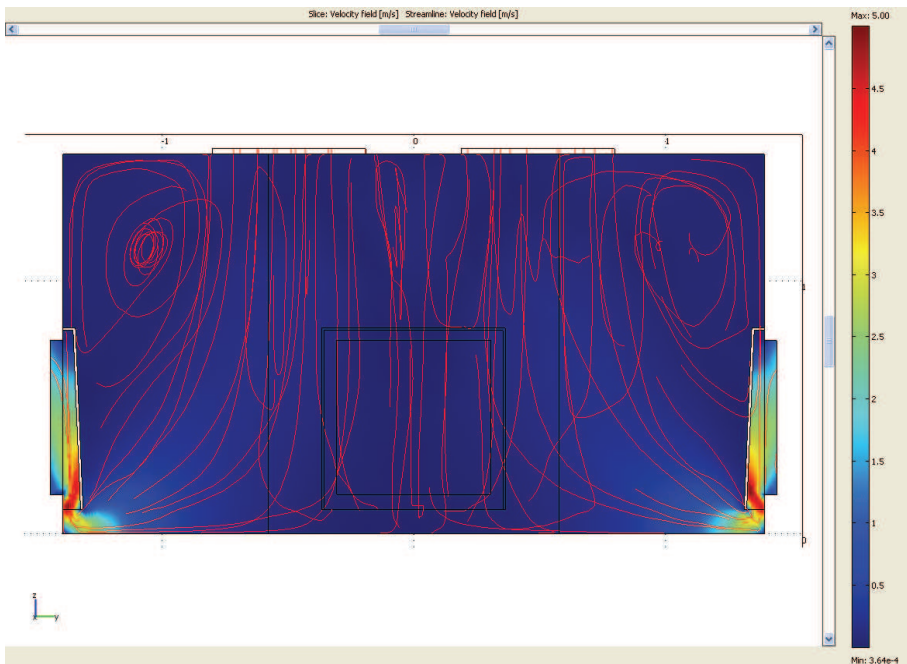


Figure 11. Simulated velocity field of the aseptic clean room at $x=0$ ($k-\epsilon$ model)

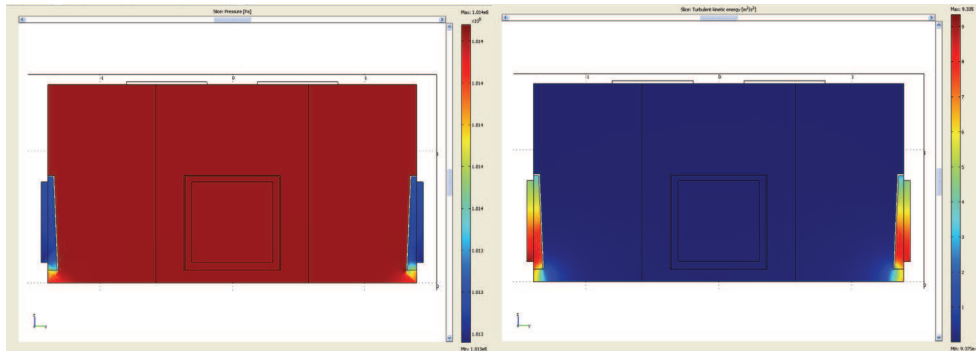


Figure 12. Simulated pressure values (a) and turbulent kinetic energy (b) of the aseptic clean room at $x=0$ ($k-\varepsilon$ model)

5. Conclusions

Contamination control has become a key factor in assuring product reliability in many high technology industries, and strictly depends on the capability to precisely control the turbulent flows of sterile air inside the container into which products are assembled.

To help manufacturers to tackle this issue at the design phase, in this work a simulation model has been developed to reproduce and analyze the flow of sterile air within a clean room for aseptic beverage bottling.

Two turbulence models were considered in developing the simulation tool, namely the $k-\varepsilon$ and the $k-\omega$, whose results were validated by comparing them to experimental measurements. The models used exploit different approaches to the turbulence problem, which result in different performance in predicting the fluid flow. Specifically, the $k-\varepsilon$ model is in general able to accurately reproduce the velocity profile observed during experimental measurements; this is particularly the case of the central area of the clean room (i.e. location A) and the outlet grid (i.e. location B). Conversely, the $k-\omega$ model seems to provide better estimations of fluid velocity when considering locations close to the chamber floor (i.e. location C), while some limitations of the model emerge when simulating the centre of the clean room (e.g. locations A and D), where the fluid reaches the free flow conditions.

On the basis of the results of the validation, as well as subsequent analyses performed, we can conclude that the $k-\varepsilon$ model developed can be usefully exploited to predict the fluid flow in real aseptic rooms, and, in particular, to design room size and equipments to improve air circulation. We thus believe that aseptic plant manufacturers could substantially benefit from our model as a possible tool to improve the performance of aseptic rooms.

Some of the limitations of the study should be mentioned. As a first point, both models adopted grounds on the Boussinesq hypothesis, which greatly simplifies the computation of Reynolds stress, thus speeding up the computation time. Moreover, such models are generally robust, and provide reliable results. However, the simplification used in the formulation of transport equations could affect the accuracy of the results provided. In particular, the Boussinesq hypothesis provides a definition of the turbulent viscosity as a scalar quantity, which implicitly suggests viscosity to be an isotropic value. Such an assumption is rarely satisfied, except for simple systems, which could not be the case of the aseptic clean room examined. Moreover, an additional source of error of two-equation

models has to be found in the assumption of direct proportion between kinetic energy k and dissipation rate ε . Such assumption can be considered as satisfied only for high Reynolds numbers. From the simulation point of view, a main limitation of the work is the number of elements used in the mesh. To improve the model accuracy, this should be increased, either by adopting segregated solvers or by increasing the computational capacity of the system.

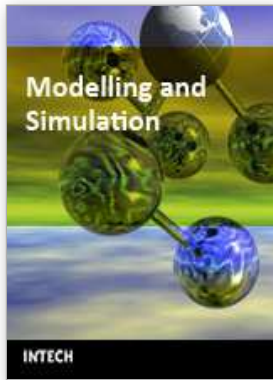
Starting from this study, future research can be directed at:

- (i) exploiting the model developed to design possible improvements for the aseptic clean room, with the ultimate aim of improving the circulation of sterile air along walls, windows and ceiling of the room;
- (ii) exploiting the model to define the hydrogen peroxide flow inside the clean room, with the aim to derive the fluid distribution in the room and to examine the corresponding sterilization performance;
- (iii) applying different turbulence models to the simulation tool developed, such as the RNG and realizable k - ε models or the k - ω SST model (Kuznik, et al., 2007), with the aim to improve the simulation results and to better predict the fluid flow in the aseptic clean room.

6. References

- Chen S.C., Tsai C.J., Li S.N., Shih H.Y. (2007). Dispersion of gas pollutant in a fan-filter-unit (FFU) cleanroom. *Building and Environment*, 42, 1902-1912
- Cheng M., Liu G.R., Lam K.Y., Cai W.J., Lee E. L. (1999). Approaches for improving airflow uniformity in unidirectional flow cleanrooms. *Building and Environment*, 34, 275-284
- Comsol Inc., (2005), *User's Guide*, Comsol Multiphysics 3.2a, Sweden
- Divelbiss J., Winter B. (1995). Isolator evaluation using computer modelling. Part 2: hydrogen peroxide sterilization with two diluents fluids. *Pharmaceutical Engineering*, 15(3), 84-96
- Favre, A. (1969). Statistical equations of turbulent gases. In Lavrentev, M.A., (Ed.), *Problems of Hydrodynamics and Continuum Mechanics*. Society for Industrial and Applied Mathematics, 0-898-71039-1, Philadelphia
- Federal Standard 209E, (2002), *Airborne Particulate Cleanliness Classes in Cleanrooms and Clean Zones*. Institute of Environmental Sciences, Illinois. Available at <http://www.set3.com/papers/209e.pdf>
- Fitzpatrick, B.W.F. (1994). Contamination control in the food industry . assembly of food components in clean rooms. *Swiss Food*, 16, 7-8
- ISO 14644-8:2006 Cleanrooms and associated controlled environments. Classification of airborne molecular contamination.
- Kolmogorov, A.N. (1941). The local structure of turbulence in incompressible viscous fluid for very large Reynold's numbers. *C. R. Dokl. Acad. Sci. URSS*, 30, 301-305
- Kuznik F., Rusaouen G., Brau J. (2007). Experimental and numerical study of a full scale ventilated enclosure: Comparison of four two equations closure turbulence models. *Building and Environment*, 42, 1043-1053
- Launder B.E., Spalding D.B. (1974). The numerical computation of turbulent flow. *Computer Methods in Applied Mechanics and Engineering*, 3, 269-289
- Ljungqvist B., Reinmuller B. (1997). *Clean room design/minimizing contamination through proper design*. Interpharm Press, 1-574-91032-9, Buffalo Grove

- Norton T., Sun D.W. (2006). Computational fluid dynamics (CFD) - an effective and efficient design and analysis tool for the food industry: A review. *Trends in Food Science & Technology*, 17(11), 600-620
- Ogawa, M. (2000). Contamination control in HVAC systems for aseptic processing area. Part I: Case study of the airflow velocity in a unidirectional airflow workstation with computational fluid dynamics. *PDA Journal of Pharmaceutical Science and Technology*, 54, 27-31
- Rajagopal K.R., Ruzicka M., Srinivasa A.R. (1996). On the Obserbeck-Boussinesq approximation. *Mathematical Models & Methods in Applied Sciences* 6, 1157-1167
- Reynolds, O. (1883). An experimental investigation of the circumstances which determine whether the motion of water shall be direct or sinuous, and of the law of resistance in parallel channels. *Philosophical Transactions of the Royal Society*, 174, 935-982
- Schicht, H.H. (1999). Cleanroom technology and its benefits to the food and beverage industry. *New Food*, 1, 18-23
- Whyte, W. (2001). *Cleanroom technology, Fundamentals of design, testing and operation*. John Wiley & Sons Ltd., 0-471-86842-6, Chichester
- Wilcox, D.C. (1988). Re-assessment of the scale-determining equation for advanced turbulence models. *AIAA Journal*, 26, 1414-1421
- Wilcox, D.C. (1998). *Turbulence Modeling for CFD*. DCW Industries Inc., 1-928729-10-X, USA
- Wirtanen, G., Miettinen, H., Pahkala, S., Enbom, S. & Vanne, L. (2002). *Clean air solutions in food processing*. Available at www.vtt.fi/inf/pdf/publications/2002/P482.pdf



Modelling and Simulation

Edited by Giuseppe Petrone and Giuliano Cammarata

ISBN 978-3-902613-25-7

Hard cover, 688 pages

Publisher I-Tech Education and Publishing

Published online 01, June, 2008

Published in print edition June, 2008

This book collects original and innovative research studies concerning modeling and simulation of physical systems in a very wide range of applications, encompassing micro-electro-mechanical systems, measurement instrumentations, catalytic reactors, biomechanical applications, biological and chemical sensors, magnetosensitive materials, silicon photonic devices, electronic devices, optical fibers, electro-microfluidic systems, composite materials, fuel cells, indoor air-conditioning systems, active magnetic levitation systems and more. Some of the most recent numerical techniques, as well as some of the software among the most accurate and sophisticated in treating complex systems, are applied in order to exhaustively contribute in knowledge advances.

How to reference

In order to correctly reference this scholarly work, feel free to copy and paste the following:

Eleonora Bottani, Roberto Rizzo and Giuseppe Vignali (2008). Numerical Simulation of Turbulent Air Flows in Aseptic Clean Rooms, Modelling and Simulation, Giuseppe Petrone and Giuliano Cammarata (Ed.), ISBN: 978-3-902613-25-7, InTech, Available from:

http://www.intechopen.com/books/modelling_and_simulation/numerical_simulation_of_turbulent_air_flows_in_aseptic_clean_rooms

INTECH

open science | open minds

InTech Europe

University Campus STeP Ri
Slavka Krautzeka 83/A
51000 Rijeka, Croatia
Phone: +385 (51) 770 447
Fax: +385 (51) 686 166
www.intechopen.com

InTech China

Unit 405, Office Block, Hotel Equatorial Shanghai
No.65, Yan An Road (West), Shanghai, 200040, China
中国上海市延安西路65号上海国际贵都大饭店办公楼405单元
Phone: +86-21-62489820
Fax: +86-21-62489821